 ©2016 Kvantovaya Elektronika and Turpion Ltd

DOI: 10.1070/QEL15993

Simulation of picosecond pulse propagation in fibre-based radiation shaping units

G.V. Kuptsov, V.V. Petrov, A.V. Laptev, V.A. Petrov, E.V. Pestryakov

Abstract. **We have performed a numerical simulation of picosecond pulse propagation in a combined stretcher consisting of a segment of a telecommunication fibre and diffraction holographic gratings. The process of supercontinuum generation in a nonlinear photonic-crystal fibre pumped by picosecond pulses is simulated by solving numerically the generalised nonlinear Schrödinger equation; spectral and temporal pulse parameters are determined. Experimental data are in good agreement with simulation results. The obtained results are used to design a high-power femtosecond laser system with a pulse repetition rate of 1 kHz.**

Keywords: *femtosecond laser, optical fibre, photonic-crystal fibre, supercontinuum, numerical modelling.*

1. Introduction

Interest in obtaining high-power laser pulses is determined by multiple applications, including the interaction of high-intensity radiation with matter, acceleration of charged particles and prospects of controlled thermonuclear fusion. Owing to significant progress in the development of high-power pump diode lasers, chirped-pulse amplification laser systems using the media doped with Yb^{3+} ions, with the energy level of several tens of joules [1], have become widespread.

At the Institute of Laser Physics SB RAS (Novosibirsk), a diode-pumped femtosecond laser system with a pulse repetition rate of 1 kHz is developed on the basis of Yb^{3+}-doped media [2]. The choice of these active media is stipulated by the possibility of using diode pumping with a high efficiency of converting current into light and precise matching of the wavelength to the medium absorption peak, which significantly reduces parasitic and thermal losses. A peculiarity of the system is the use of hybrid (parametric and laser) methods of chirped-pulse amplification with optical synchronisation of channels. The block diagram of the system is shown in Fig. 1.

After pre-amplification, radiation from a master oscillator is divided into two channels – pump channel and amplification channel. The first channel consists of two multipass amplifiers and a nonlinear-optical crystal for the second harmonic generation; the expected output pulse energy is 150 mJ. The amplification channel consists of a unit of spectral pulse broadening on the basis of a photonic-crystal fibre and a BBO-based parametric amplifier. The system is designed to produce output pulses with a repetition rate of 1 kHz, an energy of 10 mJ, and a duration of 10 fs, which corresponds to a power of 1 TW.

An $Yb:Y_2O_3$-ceramic diode-pumped master laser operates at cryogenic temperatures (near 77 K), which improves the efficiency of laser operation according to the four-level scheme by reducing thermal effects [3]. However, at liquid-nitrogen temperatures, the gain contour width is considerably reduced, which leads to generation of pulses with a spectral width (FWHM) of 1.7 nm and a centre wavelength of 1030 nm at a pulse duration (FWHM) of 2.5 ps, a repetition rate of 80 MHz and an average power of 100 mW.

2. Combined fibre-grating stretcher

According to calculations, the master oscillator radiation should be amplified in the pump channel of a parametric amplifier up to an energy level of 300 mJ to reach a terawatt power level at the system output. The calculations show that, if the pulse duration before amplification exceeds 1 ns, the peak intensity throughout the entire optical path of the amplifier is below the breakdown threshold of optical coatings and amplifier elements. Otherwise, the use of crystals with a large aperture is required, which is certainly expensive.

Grating, fibre and prism stretchers are commonly used for stretching pulses in the time domain. The spectral width of stretched pulses determines the grating stretcher dimensions (over 3 m in the case of holographic gratings with 1700 lines mm^{-1}), which provides a desired duration (1 ns). The fibre stretcher has a substantially smaller size, but it either would produce a large chirp of higher orders (due to a large pulse propagation length of $\sim$7 km) or would be costly (in the case of specialised fibres). In addition, a large propagation distance inevitably leads to undesirable significant losses

G.V. Kuptsov, E.V. Pestryakov Institute of Laser Physics, Siberian Branch, Russian Academy of Sciences, prosp. Akad. Lavrent'eva 13/3, 630090 Novosibirsk, Russia; Novosibirsk State University, ul. Pirogova 2, 630090 Novosibirsk, Russia; e-mail: kuptsov.gleb@gmail.com, pefvic@laser.nsc.ru;
V.V. Petrov Institute of Laser Physics, Siberian Branch, Russian Academy of Sciences, prosp. Akad. Lavrent'eva 13/3, 630090 Novosibirsk, Russia; Novosibirsk State University, ul. Pirogova 2, 630090 Novosibirsk, Russia; Novosibirsk State Technical University, prosp. K. Marksa 20, 630092 Novosibirsk, Russia; e-mail: vpetv@laser.nsc.ru;
A.V. Laptev Institute of Laser Physics, Siberian Branch, Russian Academy of Sciences, prosp. Akad. Lavrent'eva 13/3, 630090 Novosibirsk, Russia;
V.A. Petrov Institute of Laser Physics, Siberian Branch, Russian Academy of Sciences, prosp. Akad. Lavrent'eva 13/3, 630090 Novosibirsk, Russia; Novosibirsk State Technical University, prosp. K. Marksa 20, 630092 Novosibirsk, Russia

Received 7 December 2015; revision received 7 July 2016
Kvantovaya Elektronika **46** (9) 801–805 (2016)
Translated by M.A. Monastyrskiy

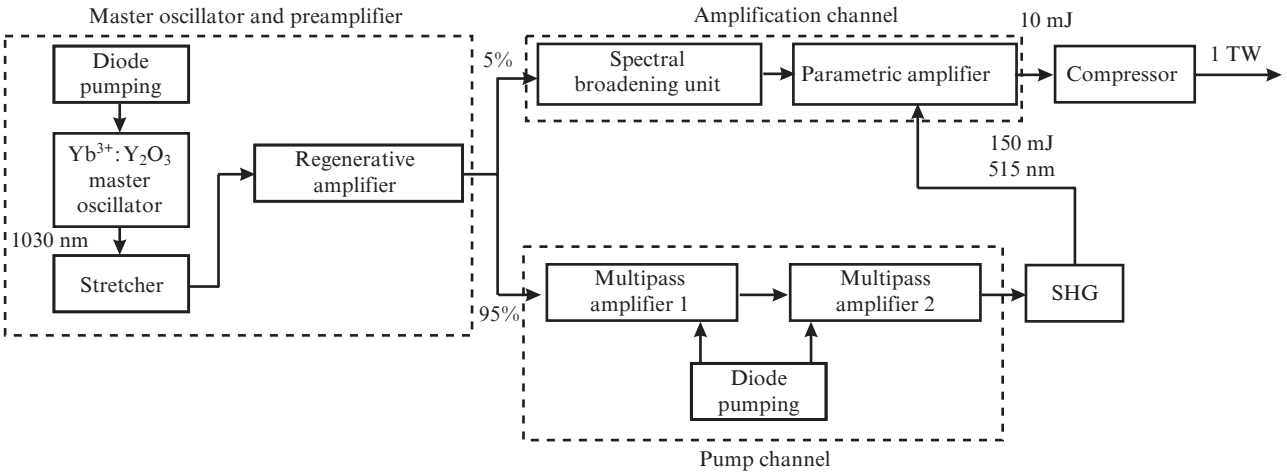

Figure 1. Layout of a diode-pumped high-intensity femtosecond laser system; the pulse repetition rate is 1 kHz.

caused by absorption and scattering in the optical fibre. The prism stretchers have a smaller dispersion than the grating ones, and thus even greater dimensions.

To address these shortcomings, we have proposed a combined stretcher consisting of fibre and grating stretchers arranged sequentially (Fig. 2). This configuration assumes the use of a short (50–150 m in the case of a standard SMF-28 telecommunication fibre) fibre section, in which the combined effect of self-phase modulation and second-order dispersion leads to the spectrum broadening with an insignificant distortion of its spectral profile. In a small-size grating stretcher (the distance along the normal between the gratings amounts to 1 m), the pulse pre-broadened by spectrum is stretched up to 1 ns.

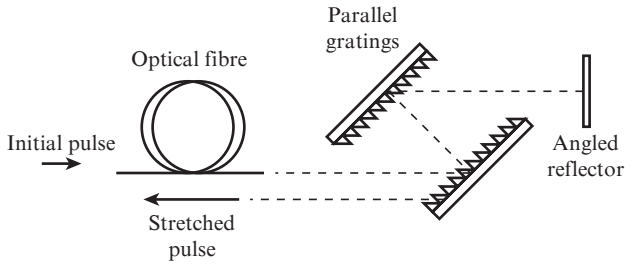

Figure 2. Layout of a hybrid stretcher.

In simulations, we have used the experimentally measured parameters of the original pulse: Gaussian pulse duration (FWHM) of 2.5 ps, peak power of 8–250 W, Gaussian spectral pulse profile with FWHM of 1.7 nm and centre wavelength of 1030 nm. The second and third orders of dispersion in optical fibre have been taken into account; the fibre stretcher length was varied in the range from 20 to 200 m. Holographic gratings with 1700 lines mm^{-1} has been selected for the grating stretcher, the angle of incidence onto the first grating was varied from 50 to 70°. The range of angles for these gratings was determined by the condition of the diffraction efficiency (over 50%) in the first diffraction order. The grating stretcher was modelled in the configuration of a double pass of radiation through a pair of parallel gratings [4].

Based on the numerical simulation method that is described below, we determined the optimal parameters of a combined stretcher: the average power launched into the fibre is 50 mW, the fibre length is 150 m, the distance between the gratings along the normal is 0.75 m and the angle of incidence on the first grating is 55°. At these parameters, the pulse duration at the combined stretcher output is 1 ns, which satisfies the task at hand, the spectral width (FWHM) is 3.1 nm. The time profile of the output pulse is shown in Fig. 3. For this pulse, the transform-limited pulse duration amounts to 480 fs.

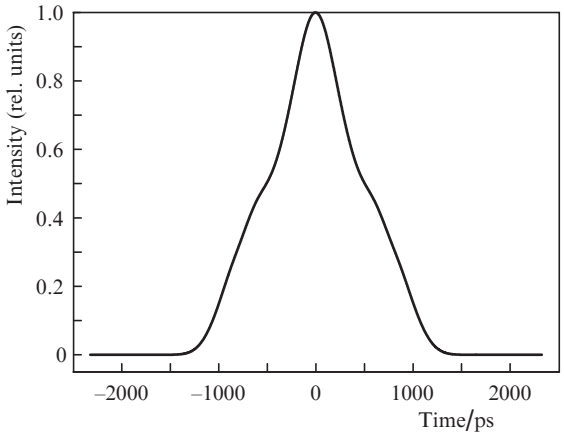

Figure 3. Temporal profile of the pulse at the hybrid stretcher output.

3. Spectral broadening in a highly nonlinear photonic-crystal fibre

The spectral width of the pulses obtained after their passage through the fibre or hybrid stretcher and amplification in a regenerative amplifier does not exceed 6 nm. This allows the propagation of pulses with a duration of ~250 fs and greater. To achieve a power of 1 TW at the system output with the same pulse energy, the spectrum should be broadened up to about 150 nm or more in the channel of parametric amplification, which corresponds to the duration of less than 10 fs at a centre wavelength of 1030 nm.

A highly nonlinear photonic-crystal SC-5.0-1040 fibre (HNPCF) (NKT Photonics) has been selected for the spectrum broadening. The fibre nonlinearity coefficient (accord-

ing to the specification) is $\gamma = 11\ \mathrm{W^{-1}\,km^{-1}}$; the zero dispersion wavelength is 1040 ± 10 nm. The choice of fibre has been stipulated by its high nonlinearity, suitable zero dispersion wavelength, sufficient radiation resistance and availability. The pulses having been pre-stretched in the time domain by means of the fibre or grating stretcher are launched from a regenerative amplifier into the HNPCF.

In the first experiment, we used a grating stretcher that stretches each pulse up to 50 ps and does not change the pulse spectra, and in the second experiment we had a fibre stretcher (the SMF-28 fibre with a length of about 2.4 km) that stretches the pulses up to 400 ps and broadens their spectra up to 6 nm (FWHM). Then, in both experiments, radiation was amplified in a regenerative amplifier and launched into a 10-m-long fibre segment using a precision three-axis table, with a microlens mounted on that table.

If the peak power launched into the fibre exceeds a certain threshold (~5 kW), super-broadening of the spectrum (supercontinuum generation) is observed [5]. The radiation spectrum wings are significantly raised with increasing input power. After reaching a peak power of about 40 kW, there occurs an optical breakdown at the HNPCF input. Figure 4 shows the spectra obtained for two different types of stretchers at the same (~30 kW) input peak power. It is seen that the use of the fibre stretcher provides a spectral shape being closer to the Gaussian profile, which is desirable for further amplification. This can be explained by the fact that the broadened spectrum is several times wider compared to the initial spectrum (6 nm versus 1.7 nm) leads to an increase in the number of frequencies involved at the early stages of the transformation processes.

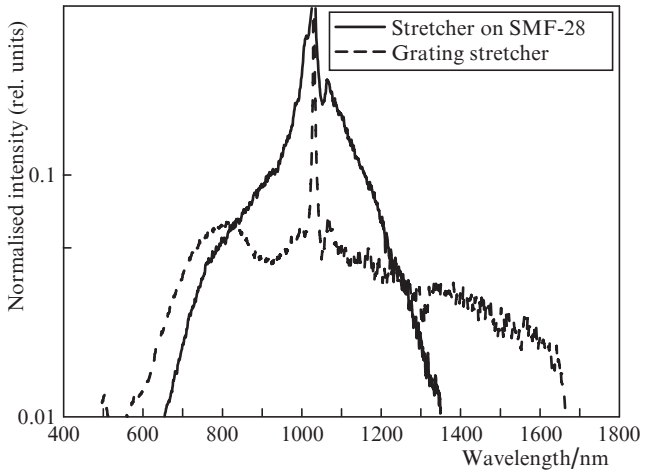

Figure 4. Experimental results obtained for two types of stretchers.

Based on the data presented, for example, in [6, 7], we may conclude that in this case the real zero dispersion wavelength for the SC-5.0-1040 fibre is slightly less than 1030 nm; therefore, the main mechanism of the HNPCF spectrum broadening is phase-matched power-dependent four-wave mixing.

The supercontinuum generation process was modelled by means of a numerical solution of the nonlinear Schrödinger equation (NSE) using a fourth-order Runge–Kutta in the interaction picture method and taking into account the internal fibre noises together with 12 first terms of the dispersion curve expansion. The line losses were not taken into account, i.e. they could be neglected because the fibre length in use was 10 m, so that the losses had no significant effect on the development of the processes.

The experimentally derived pulse parameters at the output of the regenerative amplifier were used in the calculations of supercontinuum generation: peak power of 30 kW, centre wavelength of 1029 nm, envelope width (FWHM) of 6 nm and pulse duration (FWHM) of 400 ps. The duration of pulses and their spectrum width correspond to the fibre stretcher configuration.

According to the simulation results, the spectrum of a single pulse at the HNPCF output is noisy. This is due to the fact that the parametric processes start from a seed which, in this case, represents the internal fibre noises. In the experiment, spectrometer measures a spectrum averaged by 40 pulses, while in the process of modelling the pulses with the same parameters, but with the noises different in phase, by averaging them over iterations, it is possible to obtain a smooth spectrum. The calculated and experimental spectra are shown in Fig. 5. The discrepancy between the experimental and calculated spectra can be explained by the following factors: the fibre dispersion curve provided by the manufacturer may have a qualitatively different view for a specific fibre; the accuracy of calculating the dispersion coefficients of higher orders for a curve given by the manufacturer in the form of a graph is not sufficient; the spectrometer calibration for a wide measuring range is not ideal. Nevertheless, despite some differences, the two curves have approximately the same shape, which suggests the correctness of the simulations and relevant conclusions.

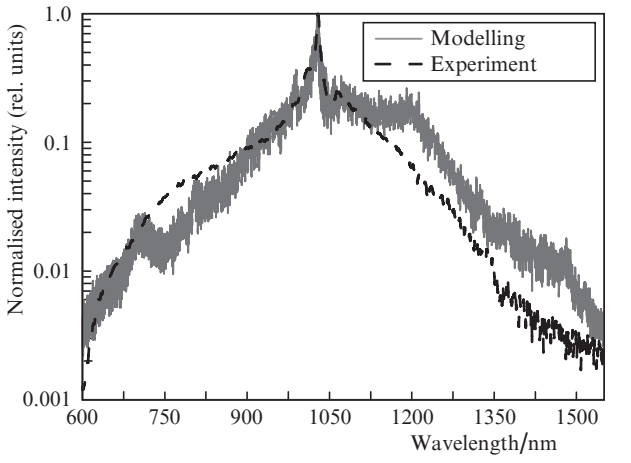

Figure 5. Spectrum at the fibre output after averaging over 40 separate pulses, and the simulation results.

4. Numerical modelling of light pulse propagation in an optical fibre

The full description of the light pulse propagation in an optical fibre requires numerical solution of the nonlinear Schrödinger equation:

$$\frac{\partial A(z,t)}{\partial z} + \frac{\alpha}{2}A(z,t) + \sum_{n\geqslant 2} \mathrm{i}^{n-1}\beta_n \frac{\partial^n A(z,t)}{\partial T^n} =$$

$$\mathrm{i}\gamma\left(1 + \frac{\mathrm{i}}{\omega_0}\frac{\partial}{\partial T}\right)\left[A(z,T)\int_{-\infty}^{\infty} R(t')\,|\,A(z,T-t')\,|^2\,\mathrm{d}t'\right], \quad (1)$$

where $A(z, T)$ is the complex amplitude of the field ($W^{1/2}$); z is the spatial coordinate (m); T is the retarded time (s); α is the fibre loss (dB km^{-1}); β_n is the group-velocity dispersion in a medium (s^n km^{-1}); γ is the fibre nonlinearity (W^{-1} km^{-1}); ω_0 is the centre frequency of the envelope (rad s^{-1}); and the function $R(t')$ is responsible for the stimulated Raman scattering associated with the instantaneous (electronic) and delayed (molecular) medium responses.

Equation (1) is a nonlinear partial differential equation which has no exact analytical solution in an arbitrary case; therefore, it is to be solved numerically. It should be noted that, for the pulses with a wide spectrum profile, the solution of the equation in frequency representation is preferable [8]:

$$\frac{\partial \tilde{A}(z,t)}{\partial z} + \frac{\alpha}{2}\tilde{A}(z,\omega) - \mathrm{i}\sum_{n\geqslant 2}\frac{\beta_n(\omega-\omega_0)^n}{n!}\tilde{A}(z,\omega) =$$

$$\mathrm{i}\gamma\Big(1+\frac{\omega}{\omega_0}\Big)F\{A(z,T)F^{-1}[\tilde{R}(\omega)F(|A(z,T)|^2)]\}, \qquad (2)$$

where F is the Fourier transform operator; F^{-1} is the inverse Fourier transform operator; and tilde denotes the Fourier transforms of respective functions.

This form of the equation follows from applying the Fourier transform to both sides of the equation [9]. In this form, the equation can be solved, for example, using the well-known split-step Fourier method. In order to improve the algorithm performance by expressing the field complex amplitude in the form

$$\tilde{C}(z,\omega) = A(z,\omega)\exp\left[z\sum_{n\geqslant 2}\frac{\beta_n(\omega-\omega_0)^n}{n!}\right] \qquad (3)$$

and substituting it into (2), we obtain the final expression in the form:

$$\frac{\partial \tilde{C}(z,\omega)}{\partial z} = \mathrm{i}\gamma\Big(1+\frac{\omega}{\omega_0}\Big)\exp\left\{-\Delta z\left[\frac{\alpha}{2} - \mathrm{i}\sum_{n\geqslant 2}\frac{\beta_n(\omega-\omega_0)^n}{n!}\right]\right\}$$

$$\times F\{A(z,T)F^{-1}[\tilde{R}(\omega)F(|A(z,T)|^2)]\}. \qquad (4)$$

Equation (3) can be integrated in one step, thereby increasing the performance. For example, the widely spread and well-studied fourth-order Runge–Kutta algorithm is applicable for integration [8]. In addition to an increase in the computation speed, the use of this algorithm allows evaluating the calculation error and automatic changing the integration step, which increases the method accuracy. The algorithm for solving the generalised nonlinear Schrödinger equation in form (4) using the fourth-order Runge–Kutta algorithm is called the interaction picture method (RK4IP) [10].

Noises play an important role in parametric processes. This is primarily due to the fact that, in the case of spectrum superbroadening, there occurs a parametric amplification of single photons, which are always present in a medium. In this work, the noises have been taken into account in the following way: the noise corresponding to one photon in the mode, with an arbitrary uniformly distributed phase, was added to the initial pulse:

$$\tilde{C}_\mu(z,\omega) = \tilde{C}(z,\omega) + \sqrt{\frac{\hbar\omega}{f_{\mathrm{rep}}}}\exp[\mathrm{i}\sigma(\omega-\omega_0)], \qquad (5)$$

where σ is a random value uniformly distributed in the range $0 < \sigma < 2\pi$. The repetition rate f_{rep} in this case is equal to the grid frequency interval of the Fourier transform.

Then, with allowance for the noises, equation (4) can be rewritten in the form:

$$\frac{\partial \tilde{C}_\mu(z,\omega)}{\partial z} = \mathrm{i}\gamma\Big(1+\frac{\omega}{\omega_0}\Big)\exp\left\{-\Delta z\left[\frac{\alpha}{2} - \mathrm{i}\sum_{n\geqslant 2}\frac{\beta_n(\omega-\omega_0)^n}{n!}\right]\right\}$$

$$\times F\{A_\mu(z,T)F^{-1}[\tilde{R}(\omega)F(|A_\mu(z,T)|^2)]\}, \qquad (6)$$

where, according to (3),

$$A_\mu(z,\omega) = \tilde{C}_\mu(z,\omega)\exp\left[-z\sum_{n\geqslant 2}\frac{\beta_n(\omega-\omega_0)^n}{n!}\right]. \qquad (7)$$

To verify the RK4IP algorithm implementation, a series of experiments was carried out, the results of which have been compared with simulation data. Experimental data were obtained for the pulses at the output of the 'master oscillator–fibre stretcher' system.

A fibre stretcher was simulated and experimentally tested for the SMF-28 telecommunication fibre; nominal specifications, with the fibre length equal to 2.4 km, were used in this simulation. In this calculation, the initial pulse parameters corresponding to those experimentally measured were used: Gaussian pulse duration (FWHM) of 2.5 ps, peak power of 8–250 W, Gaussian spectral profile of the pulse with a centre wavelength of 1030 nm and FWHM of 1.7 nm. The second and third orders of the mode-propagation constant in fibres were taken into account. The simulation results and experimental data are shown in Figs 6 and 7.

The powers launched into the fibre are determined by the discrete step of the diffractive power attenuator which does not change temporal and spectral characteristics of the pulse. It is seen that both calculated and experimental curves are in good agreement, which leads to a conclusion about the correctness of the RK4IP algorithm implementation and indicates the opportunity of numerical evaluation of the output radiation parameters depending on the known input parameters and material parameters of the optical fibre.

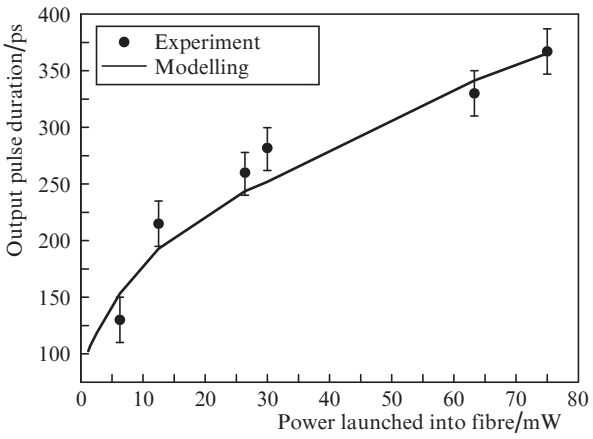

Figure 6. Pulse duration at the fibre output as a function of the lauched average power.

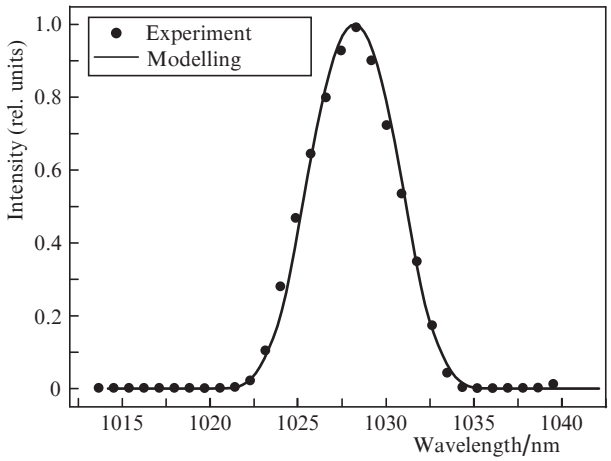

Figure 7. Experimental and simulated spectral profiles at the SMF-28 fibre output for a peak power of 250 W.

5. Conclusions

On the basis of the implemented and experimentally verified RK4IP algorithm, we have solved numerically the NSE by a fourth-order Runge–Kutta in the interaction picture method, and then simulated the hybrid fibre-grating stretcher and the process of supercontinuum generation in the HNPCF.

In accordance with the simulation results, optimal parameters of a combined stretcher have been determined. It is shown that, in the fibre part of the combined stretcher, owing to simultaneous action of the self-phase modulation and second-order dispersion, the spectrum broadening with a nearly-Gaussian profile is observed. In turn, the grating part of the combined stretcher introduces dispersion effects, which, with allowance for the initial spectrum broadening, allows us to achieve the required output pulse duration.

A unit for the spectrum broadening, based on the SC-5.0-1040 HNPCF, has been designed and developed. A supercontinuum has been experimentally obtained and the process of its generation in a highly nonlinear photonic-crystal fibre has been numerically simulated. The obtained and experimental data are in agreement. In accordance with the results of simulation, it is shown that the duration of transform-limited pulse, calculated by the pulse spectra at the fibre output, does not exceed 5 fs. The radiation can be used for further amplification in the parametric amplification channel of the femtosecond terawatt laser system.

Acknowledgements. The authors thank A.V. Kirpichnikov for assistance. The research was supported by the programmes of the Presidium of the Russian Academy of Sciences 'Extreme laser radiation: physics and fundamental applications' and the Siberian Branch of the Russian Academy of Sciences (01201374306).

References

1. Sielbold M., Hein J., Hornung M., Podleska S., Kaluza M.C., Bock S., Sauerbrey R. *Appl. Phys. B*, **90**, 431 (2008).
2. Petrov V.V., Pestryakov E.V., Petrov V.A., Kuptsov G.V., Laptev A.V. *Laser Phys.*, **24** (7), 074014 (2014).
3. Petrov V.V., Pestryakov E.V., Laptev A.V., Petrov V.A., Kuptsov G.V., Trunov V.I., Frolov S.A. *Kvantovaya Elektron.*, **44** (5), 452 (2014) [*Quantum Electron.*, **44** (5), 452 (2014)].
4. Treay E.B. *IEEE J. Quantum Electron.*, **5** (9), 454 (1969).
5. Kuptsov G.V., Petrov V.A., Laptev A.V., Petrov V.V., Pestryakov E.V. *Proc. 16th Intern. Conf. Laser Optics* (IEEE, 2014) p. 305.
6. Dudley J., Genty G., Coen S. *Rev. Mod. Phys.*, **78**, 1135 (2006).
7. Wadsworth W., Joly N., Knight J., et al. *Opt. Express*, **12**, 299 (2004).
8. Francois P.L. *J. Opt. Soc. Am. B*, **8**, 276 (1991).
9. Sinkin O.V., Holzloehner R., Zweck J., Menyuk C.R. *J. Lightwave Technol.*, **21**, 61 (2003).
10. Hult J. *J. Lightwave Technol.*, **25**, 3770 (2007).